


Chapter 10

Spatiotemporal Analysis of the Karakoram Dynamics: A Case Study of the Ghulkin Glacier, Gilgit Baltistan, Pakistan



Muhammad Amin and Aqil Tariq 

Introduction

A glacier is a big, slow-moving mass of thick ice that slides downhill. A glacier's upper half is known as the accumulation (input) zone, and it is here that snow and ice are added to the glacier by compression and snowfall. Ablation (output) zone describes the bottom part of the glacier where ice is lost due to melting and evaporation (Majeed et al., 2023). An equilibrium line of height separates the ablation and accumulation zone, where the annual balance between accumulation and ablation occurs (Esmaeili et al., 2024). Research on mass balance is critical for understanding glacial responses to recent climatic changes (Jalayer et al., 2023; Sharifi et al., 2022a), particularly how an increase in temperature and humidity causes more melting of the glacier and the formation of new glacier lakes, which results in a decrease in a glacier's mass (Basharat et al., 2022; Tariq et al., 2023). Simulation models imitate complex meteorological, glaciological, periglacial, and hydrological interactions (Basharat et al., 2022; Bokhari et al., 2023; Tariq et al., 2023). Simulating glacier dynamics at a regional scale, however, requires the adoption of "direct" approaches (e.g., in glaciological and budget methods) to meet model calibration requirements over large distances and on a longer timescale (Imran et al., 2022; Sharifi et al., 2022b; Tariq et al., 2023b; Tariq & Qin, 2023;

M. Amin

Institute of Geo-Information & Earth Observation, PMAS Arid Agriculture University
Rawalpindi, Rawalpindi, Pakistan

A. Tariq (✉)

Department of Wildlife, Fisheries and Aquaculture, College of Forest Resources, Mississippi
State University, Mississippi State, MS, United States

State Key Laboratory of Information Engineering in Surveying, Mapping and Remote Sensing,
Wuhan University, Wuhan, China

e-mail: at2139@msstate.edu; aqiltariq@whu.edu.cn

Zamani et al., 2022). Such labor-intensive approaches have not been considered practical for poorly surveyed rugged areas of glaciated ranges such as Himalaya Karakoram and Hindu Kush (HKH) (Baqa et al., 2022; Majeed et al., 2022b; Moazzam et al., 2022), which are melting at a fast rate due to local and global warming (Hussain et al., 2022a; Khan et al., 2022; Shah et al., 2022).

Among the HKH glaciers, the Karakorum glaciers in Pakistan are greatly affected by high incoming radiations, humid conditions, and heatwaves (Ghaderizadeh et al., 2022; Tariq et al., 2022b, c; Wahla et al., 2022). This is due to the increase in glacial lake formation trends during recent years, which include a high frequency of avalanches, landslides, and outburst floods from the new glacial lakes, termed glacial lake outburst floods (GLOFs). All these pose continuous hazards to the lowland communities (Fu et al., 2022; Haq et al., 2022; Jalayer et al., 2022; Majeed et al., 2022a). Understanding the current shifts in glaciers' mass balance and the resulting risks is hampered by a lack of yearly and seasonal data on glaciological observations (such as land cover changes, debris, glacial lakes, and climate factors) (Bera et al., 2022; Hussain et al., 2022b; Khalil et al., 2022b; Tariq et al., 2022a; Ullah et al., 2022).

For broad areas where field-based glaciological measurements are scarce, remote sensing (RS) has become increasingly popular due to its high spatial and temporal resolution, which allows for the estimation of glaciological mass balance and hydrometeorological changes (da Silva Monteiro et al., 2022; Islam et al., 2022; Khalil et al., 2022a; Tariq et al., 2022d). Mainly, it has been effective for real-time glacier monitoring concerning the regional and local climate. To estimate changes in the glacier surface, i.e., retreat, advance, and glacier lakes, several remote sensing techniques have been used, such as the Normalized Differentiate Water Index (NDWI) to detect the glacier lake and the normalized difference snow index (NDSI) for snow cover changes (Baloch et al., 2021; Khan et al., 2022; Majeed et al., 2021; Shah et al., 2022). In addition to that, these indicators assist in the evaluation of the hydrometeorological limits in order to estimate dangers such as GLOFs (Felegari et al., 2021; Mousa et al., 2020; Sharifi et al., 2021; Tariq, 2023).

The study aims to analyze spatiotemporal changes in the Ghulkin glacier concerning climate change that has been taking place since 1990. To do so, (i) extensive field surveys have been conducted in the Ghulkin region to estimate ice mass/volume losses at the glacier ablation zone, (ii) RS data has been used to estimate changes in the glacial land cover due to climate change, and (iii) the glacial mass losses due to climate change have been projected. The findings of this study show that from 1990 to 2015, there has been an increase in surface temperature and glacial lake formation at high altitudes and a decrease of ice mass from the side moraine at the ablation zone Ghulkin glacier.

Materials and Methods

Study Area

The research area encompasses the entirety of the Ghulkin glacier and the Hussaini settlement in the upper Hunza valley (Fig. 10.1). The latitude of the research region is 5.8026°N, and the longitude is 74.9832° E. The glacier has a total area of 28.5 km² in its entirety. The Ghulkin glacier is about 17 km long and approximately 70 m wide. The glacier ablation zone is about 6 km long, but varies with time. The glacier snout is advanced due to its steep slope, while the tendency of glacier lake formation has increased, and the ice mass from side moraines has decreased. The GLOF events are occurring more frequently in HKH glaciers, and the emergence of glacial ablation zones is the evidence (Felegari et al., 2023; Hu et al., 2021; Siddiqui et al., 2020). The Gulkin glacier is approximately 17 km in length and 70 m in width. The settlement of Hussaini can be found on the glacier’s northern flank, while the village of Gulkin can be found on its southern flank. The Karakoram Highway and the Upper Hunza River can be found to the east, and the glacier’s source peak can be found to the west.

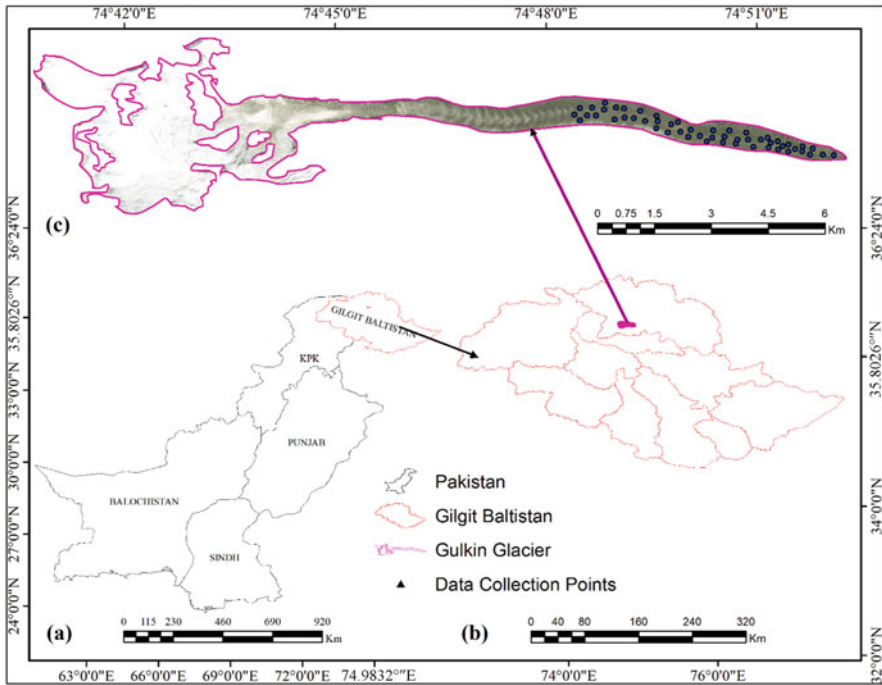


Fig. 10.1 (a) Boundary of Pakistan; (b) Gilgit Baltistan; and (c) description of the study area and data collection points at the ablation zone of Ghulkin glacier

Table 10.1 Historical GLOF events from Ghulkin Glacier

Year	Date of event	Glacier (GLOF) location	River
2007	05-April	Gulkin	Hunza
2009	03-May		
2010	04-April		
2011	28-April		
2012	14 May		
2014	27-May		

The glacier's melting zone extends for approximately 6 km in length. It has been noted that the glacier is melting at an alarming rate; this can be deduced from the appearance of supraglacial lakes that have formed in the ablation zone. It is observed that five lakes have been included in the glaciers. The construction of lakes on the glacier is so that two lakes, namely Ashore Baig and Ghowj, are on the northern side toward Hussaini village at an elevation of 2734 m and 2876 m, respectively. Ashore Baig is 200 m long and 20 m wide; its depth reaches up to 15 to 20 m, while other lakes, namely Roud 1 and 2 are located at an elevation of 2856 m in the southern side toward Gulkin village (Asif et al., 2023; Shah et al., 2021; Tariq & Shu, 2020). The average length of these two lakes is 40 m and 30 m, respectively, while the width is 25 and 20 m, respectively. These lakes show the formation of supraglacial lakes on glacier relatively oval shape, and the depth reaches up to 10 m when filled. The critical point is that all these lakes are formed near the lateral moraines of the glacier's left and right flanks. The lakes have been developed in the ablation zone, where melting is rapidly increasing (Basharat et al., 2022; Tariq et al., 2023, 2023a). The debris layer covers glaciers also washed out; this can also activate the melting rate. In the terminus point of the glacier, medium to large craves have been developed. These crevasses squeeze in winter. It reopens when temperature increases (freezing and thawing) and gives way to the flow of melting water. On the Hussaini side near the Ashore Baig lake, the crevasse is traversed in North-East (NE), and the melting flows into Ashore Baig Lake. In the same line, another lake, Ghowj, is located at a distance of 1 km upstream. From this lake, a large crevasse is observed to pass toward the Gulkin side in the direction of North to South East (N-SE) (CERT monitoring team). A parallel crack in the order of NS is also evident toward Gulkin near the terminus (see Fig. 10.4). Lateral moraines on either side of the glacier also spark evidence of the glacier's melting. It is observed that the moraines are exposed to 10 to 14 m high, while at the head of the Gulkin village, the moraines are superimposed by the glacier as the moraines are subsiding/sliding down due to the pressure of the glacier, as a result of that the moraines are diminishing and seepage from the glacier.

The villages of Sosot and Khalti in Tehsil Gupis were hit by two GLOFs in 1999. The Shimshal valley was the site of GLOF incidents in 2000. Six GLOF episodes, all originating from the Ghulkin glacier between 2007 and 2009 (Table 10.1), caused extensive damage to the Karakoram highway and local property. In 2009, the Passu glacier was responsible for one GLOF occurrence. Hundreds of trees were destroyed in 2012 due to a GLOF event that originated from the Ghulkin glacier. As a result,

the number of GLOF incidents in the region has increased since 2007, especially those caused by HKH glaciers like the Ghulkin glacier (Mihalcea et al., 2008). Therefore, the spatiotemporal effects of climate change on the Ghulkin glacier's mass balance and the accompanying hazards must be studied.

Data Sets

Remote Sensing Data

Satellite imagery of Landsat were obtained from the NASA-EROS for the years 1990, 1995, 2000, 2010, and 2015 (Table 10.2). Moreover, four spectral bands with a 30-m spatial resolution of Landsat-8 were used to cover the 1990–2015 time periods (Quincey et al., 2009). The geometric and radiometric errors were removed through pre-processing techniques before utilizing the data for image analysis.

Elevation Data

This research used the digital elevation model (DEM) data of Alospalsar, which was obtained from the NASA (Round et al., 2017). Recent research have made extensive use of the data provided by the Alospalsar DEM instrument in order to investigate spatiotemporal differences in glaciers in relation to variations in the climate of the Himalayan ranges (Pimentel & Flowers, 2011). High-resolution DEM data, in comparison to low-resolution ASTER DEM, was used to perform the following glaciological measurements on the Ghulkin glacier: calculating the total mass-loss volume at the glacier ablation zone and creating the slope and aspect surfaces for predicting the glacier mass-loss areas due to climate change.

Table 10.2 Image data specifications of Landsat-5 thematic mapper (TM), Landsat-7 enhanced thematic mapper plus (ETM+), and Landsat-8 operational land imager

Data acquisition	Satellite	Sensor	SR	TR	Path	Row	Source
22/7/1995	Landsat-4 and -5	TM	30 m	16 days	150	35	USGS (EROS)
2/7/2000	Landsat-4 and -5	TM	30 m	16 days	150	35	
17/7/2005	Landsat-7	ETM+	30 m	16 days	150	35	
14/7/2010	Landsat-7	ETM+	30 m	16 days	150	35	
14/7/2015	Landsat-8	OLI/TIRS	30 m	16 days	150	35	
11/11/2010	DEM	Aster	30 m				Earth Data

DEM digital elevation model, *ETM+* enhanced thematic mapper plus (ETM+), *OLI* operational land imager, *SR* spatial resolution, *TM* thematic mapper, *TR* temporal resolution

Mass Balance Data

With the help of the ICIMOD, its geologists, and the community watch group (CWG), accurate mass-balance data for the Ghulkin glacier's ablation zone was gathered through the use of GPS and Rangefinder. FOCUS Pakistan established the CWG group in 2008 to monitor glacier changes in Gilgit-Baltistan and Chitral under the project co-funded by ICIMOD. Data collected for 36 heights of side moraines on the left and right of the glacier is shown in Fig. 10.1.

Methods

Glacier Volume Calculation

Using direct measurements (obtained through GPS and Rangefinder), the total volume/mass loss was estimated at the glacier ablation zone. First, the inverse distance weighted (IDW) interpolation method was used to generate the mass-loss surface from the glacier's 36 mass-loss measurements. The mass-loss interpolated surface was converted into the triangular irregular network (TIN) using heights in the GPS-based field data to calculate volume loss at the glacier ablation zone. The TIN data structure allows for the inclusion of information about each pixel's x , y , and z values, which are required to calculate two- and three-dimensional areas and three-dimensional volumes. Finally, the derived TIN data was used to calculate glacier mass loss from the moraines' sides. These glacier mass losses from moraine sides were validated using field photographs collected by FOCUS Pakistan geologists and CWG members. Furthermore, the TIN surface was used to calculate the total mass-loss volume at the glacier ablation zones through the functional surface tool of three-dimensional extensions in the ArcGIS environment.

Estimating Land Cover Change of the Ghulkin Glacier

Remote sensing images were analyzed for the delineation of water bodies at the ablation zone of the glacier and the land cover classification for estimating spatio-temporal changes in the debris and water bodies from 1990 to 2015. At the same time, extractions of surface temperatures were also recorded.

Delineation of Water Bodies at the Ablation Zone of the Glacier

Landsat 4, 5, 7, and 8 images were stacked, and the NDWI was calculated as $NDWI = (Green - NIR / Green + NIR)$, where NIR is the near-infrared band of Landsat images of 4, 5, 7, and 8. The threshold value is accurately segmented as 0.4 as this threshold of NDWI values represents water bodies; therefore, they were used

to delineate temporal glacial lakes between 1990 and 2015. In addition, the segregation of the resulting images for glacial lakes was performed by correlating them with field pictures from 2007 to 2016 which were obtained from the FOCUS Humanitarian Assistance, Pakistan.

Land Cover Classification of the Ghulkin Glacier

Land cover maps of 1990 and 2015 were prepared using image classification techniques. To perform supervised classification, training data was collected from field surveys by collaborating with geologists. In total, 36 ground control points were observed from the glacier ablation zone between 2008 and 2015. Three land cover classes were mapped, including snow cover, debris, and lake waters. These classes were manually delineated with Google imagery to calculate an accurate area of each land cover class. Finally, NDWI maps were used to delineate recently formed glacial lakes. Statistics obtained from land cover maps were used to compare area changes in the glacier snow, debris, and glacier lakes between 1990 and 2015. The results of the NDWI maps were validated through high-resolution Google imagery.

Extraction of Surface Temperature on the Ghulkin Glacier

For the same period 1990–2015, thermal bands of Landsat 4–8 were used to extract temporal variations of the surface temperatures on the Ghulkin glacier. Initially, the top-of-atmosphere (TOA) radiance was extracted from the reflectance values. Equation (10.1) was rendered as follows.

$$T = K_2 / (\ln(1 + K_1 \text{ (radiance)})) - 273.15 \quad (10.1)$$

where T is at-satellite brightness temperature (Celsius), K_2 denotes the specific constant band for thermal conversion from the metadata ($K_2_CONSTANT_BAND_x$, where x is the band number), and K_1 is the band-specific constant for thermal conversion from the metadata ($K_1_CONSTANT_BAND_x$, where x is the band number). The spectral radiance is calculated as in Eq. (10.2):

$$(((L_{\max} - L_{\min}) / 254) * (DN - 1)) + L_m \quad (10.2)$$

where the values are provided in the Landsat metadata file.

Table 10.3 Weights assigned to various inputs in the weighted overlay analysis for identifying the extensive mass-loss (snow melting) areas of the Ghulkin glacier due to climate change

Inputs	Input values	Weights
Slope	0–20	9
	20–30	6
	Above 30	1
Aspect	South East	9
	East	8
	Another slope aspect	1
Predicted mass-loss	Above 15 feet	9
	10 feet	6
	Below 5	3
NDWI	0.3 above	9
	0 to 0.3	6
	Below 0	0

Weighted Overlay Analysis

Weighted overlay analysis was performed to identify the potential site for newly formed glacier lakes. We have used four datasets in raster format, namely slope, aspect, NDWI, and interpolation surface of mass loss from the side moraine of the Ghulkin glacier. These raster surfaces were reclassified and the weights were assigned in the ArcGIS environment. The consequences (0–9) for the four surfaces are shown in Table 10.3.

Results

Volume/Mass Loss at the Ablation Zone of the Ghulkin Glacier

Figure 10.2a shows the mass-loss surface of the Ghulkin glacier interpolated from the glacier's 36 mass-loss measurements. Comparing the mass-loss sites with field photographs of the ablation zone during the years 2009, 2011, 2012, and 2013 in Fig. 10.2b indicates that the ablation zone of the glacier has lost significant glacier mass (through snow melting), which developed into new water bodies on the glacier surface. The ablation zone of the glacier had losses of 163,853 cubic meters of glacier ice mass from the side moraine of the glacier. This can be viewed from landscape changes in the aerial imagery from 2009, 2011, 2012, and 2013 (see Fig. 10.2b).

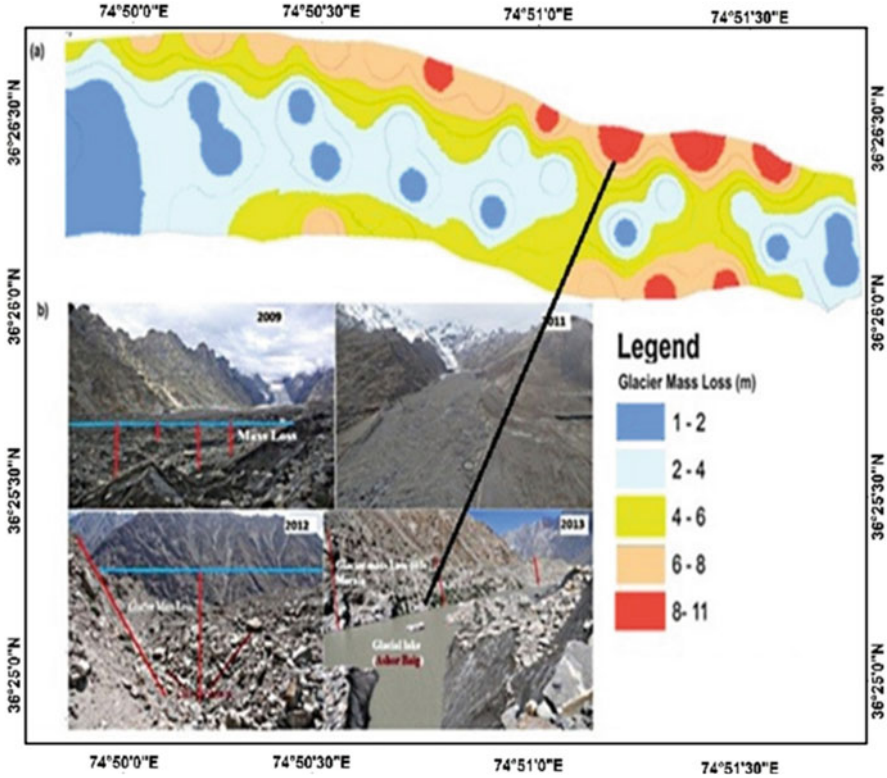


Fig. 10.2 (a) Map showing mass loss (meters) at the ablation zone of the Ghulkin glacier and (b) the field photographs of the ablation zone in 2009, 2011, 2012, and 2013

Estimating Land Cover Change of the Ghulkin Glacier due to Climate Change Through Remote Sensing

Figure 10.3 shows the temporal maps of NDWI for the period 1990 and 2015, derived from Landsat 4, 5, 7, and 8 data. The glacier lake area/size results were also validated through high-resolution Google imagery. Figure 10.4 shows spatiotemporal changes in the glacier lakes of the Ghulkin glacier in the years 1990, 1995, 2000, 2010, and 2015. This indicates that the total area covered by Ghulkin lakes has increased by 18,990 km² from 1990 to 2015. The surface temperature of the glacier has also increased between 1990 and 2015. This is undeniable evidence of the effects of global warming on glacier mass balance, the formation of high-altitude glacier lakes, and the progression of the snow line into the accumulation zone.

Figure 10.5a, b show the land cover change of the Ghulkin glacier from 1990 to 2015. This indicates that the fresh snow covered 87.17% of the glacier in 1995, and this was reduced to 82.68% in 2015 (i.e., a snow loss of 4.49% in the last 25 years).

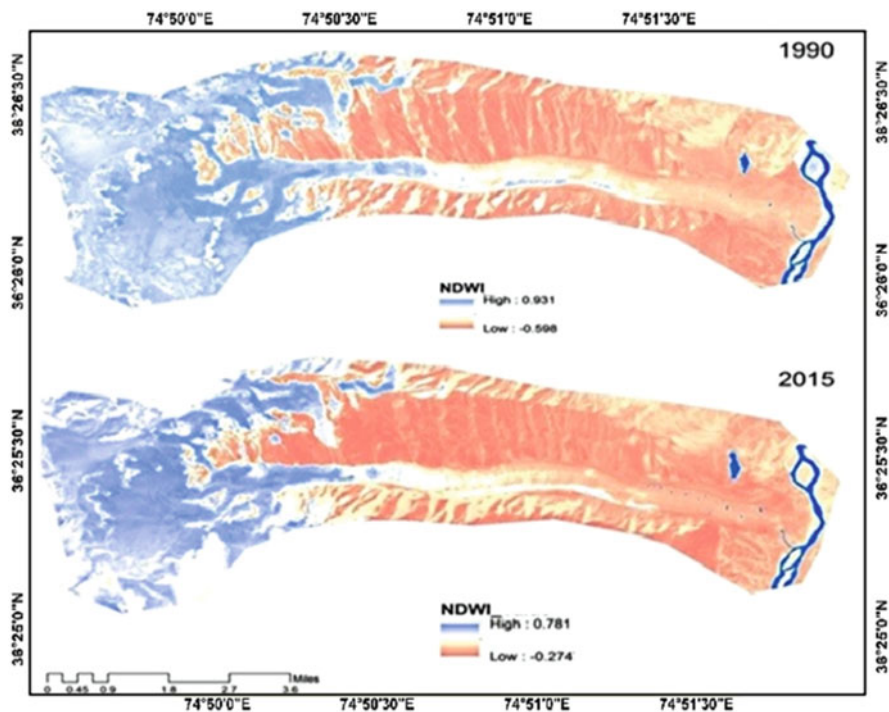


Fig. 10.3 Temporal maps of the NDWI for the period 1990–2015 derived from Landsat 4, 5, and 8 data

Consequently, the total area of the Ghulkin glacier (i.e., glacier and snow cover) decreased from 24.84 to 23.56 km² from 1990 to 2015 (see Fig. 10.5b). The snow line uplifting at a higher altitude was due to the increase in temperature. This can be seen in an increase in the debris cover on the glacier from 12.82% to 17.26% (i.e., a rise of 4.44%). The 0.005 km² area of glacier lakes in 1990 increased to 0.018 km² by 2015 (Fig. 10.5b).

Figure 10.6 shows the temporal variation of surface temperatures on the Ghulkin glacier extracted from the thermal bands of Landsat-4 and -8 for the same period (1990–2015). Clearly, this increase in temperature explains the increase in the formation of new glacier lakes during this period. A temperature increase of about 1 to 2 °C is observed locally, particularly at the ablation zone of the glacier from 1990 to 2015, compared to a global temperature increase of 0.8 °C for the same period (Lutz et al., 2014). Figure 10.7 compares locally varying surface temperatures of the Ghulkin glacier for the years 1990 and 2015. The blue line indicates 1990 data, while the red line shows the data for 2015.

This graph shows the comparison of area coverage of temperature between 1990 and 2015. In 1990, the temperature range -19 to -1 °C covered 2365.3 acres of the glacier, 0 °C covered 1501 acres, and $+1$ to $+27$ °C covered 2621.1 acres, while in

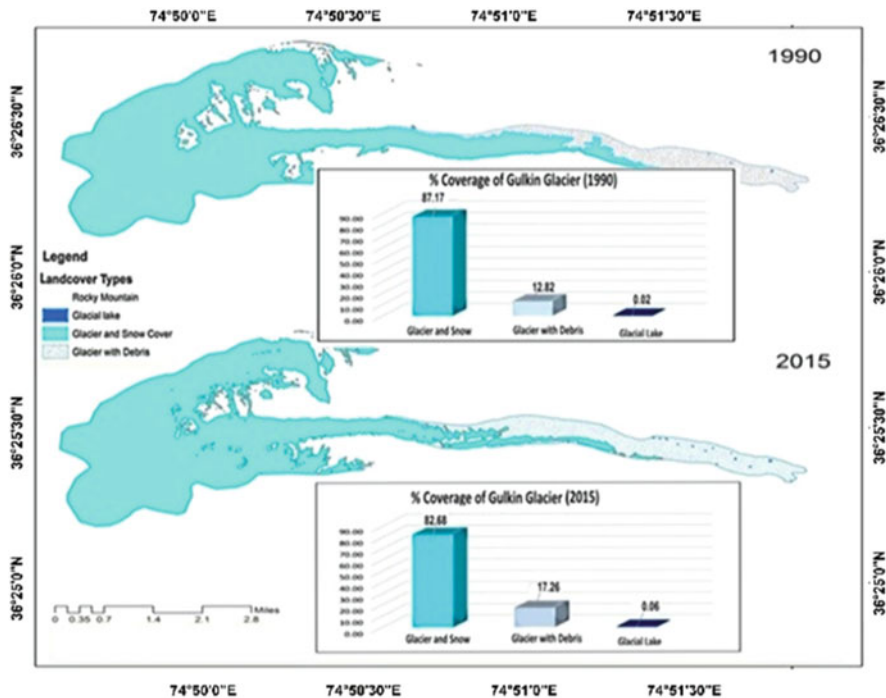


Fig. 10.4 Spatiotemporal changes in the areas of the Ghulkin glacial lakes (in sq. m) between 1990 and 2015

2015, the temperature range -19 to -1 °C covered 1645.3 acres of glacier, 0 °C covered 1623.2 acres, and $+1$ to $+27$ °C covered 3218.9 acres. The results show a significant temperature change with respective area coverage between 1990 and 2015.

Topographic Analysis of the Ghulkin Glacier

Figure 10.8 shows the results of a weighted overlay analysis of the Ghulkin glacier mass loss. The areas within the brown to red zones (5–7) have a higher probability of developing new glacier lakes due to extensive snow-cover loss in the ablation zone. The yellow zones with a value of 4 have a moderate likelihood of such change. The greener zones (within a range of 0–3) have a very low probability of changing the glacier ablation zone into glacier lakes.

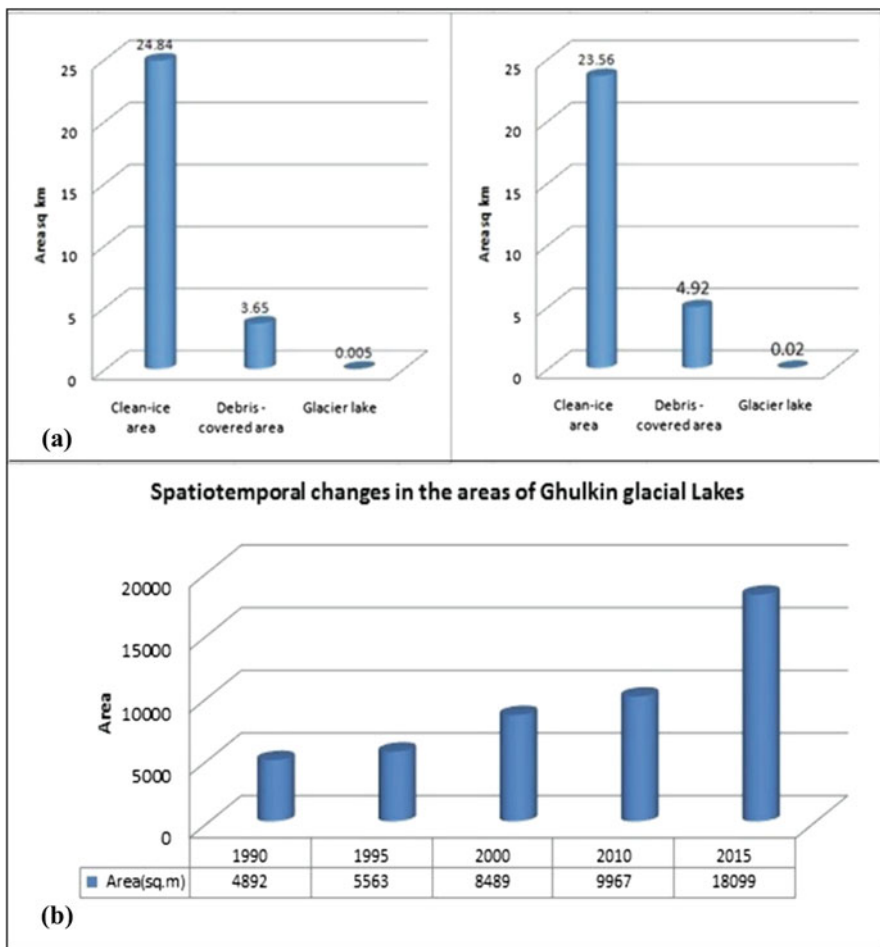


Fig. 10.5 (a) Land cover classification of percentage coverage of glacier snow, debris, and glacial lakes in 1995 and 2015 and (b) comparison of statistics for clean ice area, debris cover area, and glacial lakes in 1995 and 2015

The slope map in Fig. 10.9a shows that the ablation zone of the Ghulkin glacier existed within the range of 0–26 degrees. This is a moderate slope which is favorable for the formation of glacier lakes. The aspect map in Fig. 10.9b shows the slope directions of the glacier. The central part of the ablation zone has an east, southeast, and south aspect. These aspects have a higher tendency of solar insolation in comparison to a north slope aspect. These topographic factors clearly show that there is a greater chance of glacier lake formations.

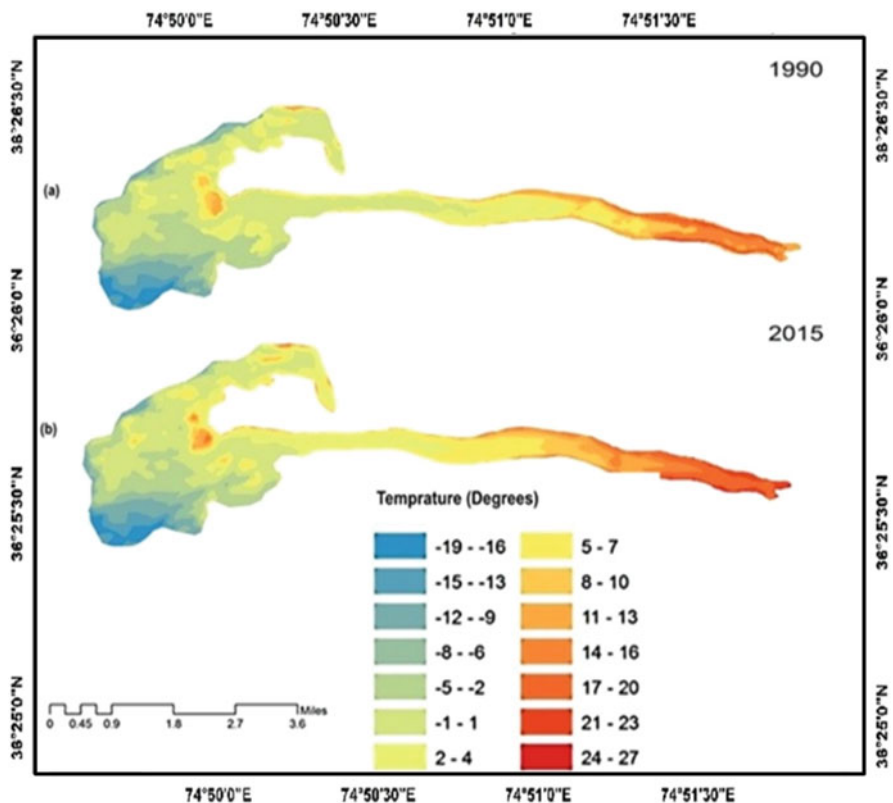


Fig. 10.6 Spatiotemporal distribution of the land surface temperatures in 1999 and 2015 derived from Landsat-4 and 8 thermal bands (TIRS)

Discussion

This study assessed the impact of climate change on the Ghulkin glacier’s mass balance by using remote sensing techniques coupled with field measurements. Such mass-balance estimations are often carried out using (1) volume-area scaling techniques that infer ice volume from the glacier area through scaling relationships (Quincey et al., 2011), (2) RS geodetic methods, which estimate changes in elevation using DEMs on a pixel-by-pixel basis; and (3) accumulation area ratio (AAR) or equilibrium line altitude (ELA) methods, which infer yearly balances of mass from two parameters associated to a glacier’s mass balance; AAR and ELA were calculated from field observations or satellite imagery. To estimate the glacier’s mass balance on the scale of the region, the ELA technique is used with field data to determine the glacier’s annual mass balance variation.

To delineate debris cover of the Ghulkin glacier, ASTER-derived DEM and field photographs were used to generate training data for the land cover classification. This is because the presence of debris cover poses problems in the image

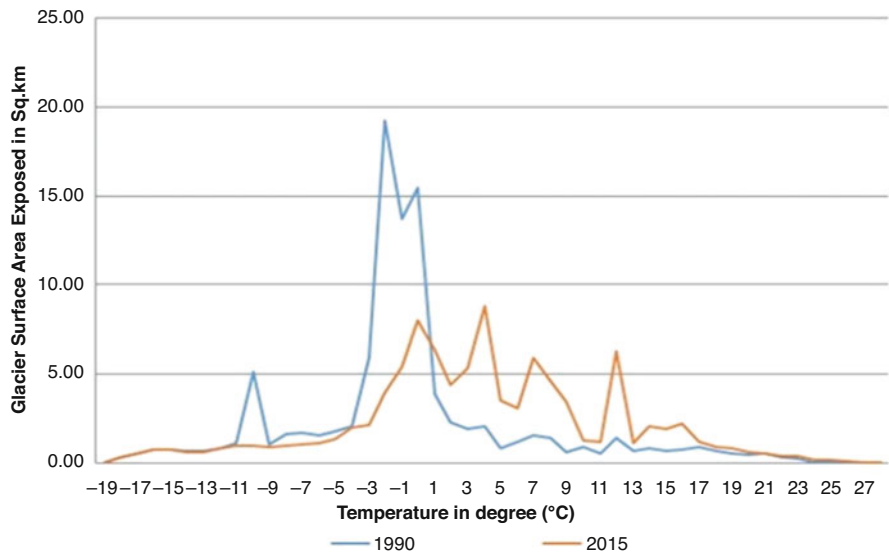


Fig. 10.7 Comparison of temperature statistics derived from Landsat images for the years 1999 and 2015

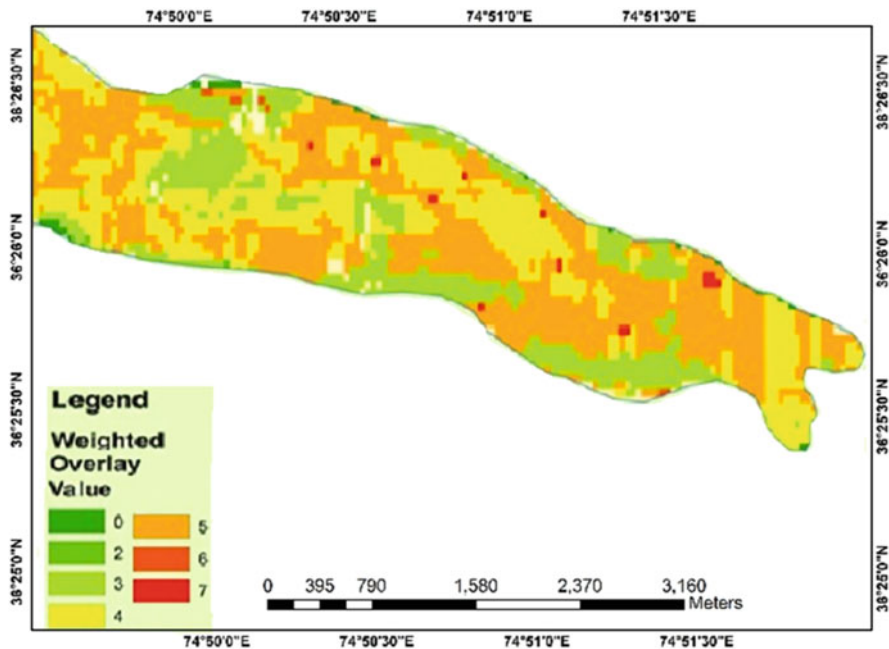


Fig. 10.8 Projected mass-loss of the Ghulkin glacier calculated using weighted overlay analyses of the slope, aspect, the NDWI, and mass-loss interpolation surfaces

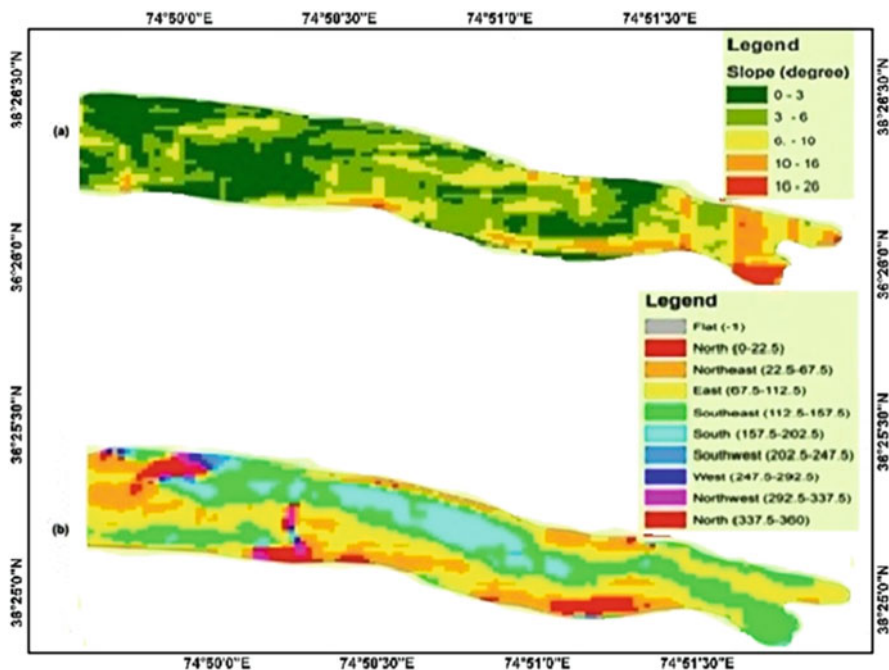


Fig. 10.9 Maps of slope (a) and aspect (b) of the ablation zone of the Ghulkin glacier

classification, and therefore in the automatic mapping of the glaciers. Moreover, widespread debris cover on HKH glacial ranges reduces their retreat rates, which are inappropriate as indicators of recent climate change (Quincey & Luckman, 2014). Nevertheless, the volume-area scaling techniques are not able to take into account such debris cover effects.

In addition to the link to changes in glacier measurements, further experimentation with this approach is needed to assess the impact of climatic variables on the mass balance of the Ghulkin glacier. This should include the following: (1) evaluating soil types to investigate further the impact of changes in debris cover on the glacier movement, (2) using other climatic parameters such as precipitation along with utilizing runoff data which could be helpful for better estimation of glacier lakes and GLOFs, and (3) coupling field data with high-resolution imagery which may be helpful to include the effect of localized seasonal variations over low-lying areas.

An important motivation for this study was to project GLOF sites over the Karakoram ranges in northern Pakistan. Using the multitemporal earth observation data, the area of the Ghulkin glacier lakes was found to have increased from 0.0065 km² to 0.02 km² between 1990 and 2015. Consequently, the devastating GLOF trend that started in 1999 continues under the present climate conditions. Our future work will extend this approach to model GLOF sites that will affect human settlements shortly.

Conclusion

The spatiotemporal analysis reveals that there has been a decrease in the overall glacier mass. During the last 25 years, the total clean-ice area decreased by 4.51%. This glacier mass loss caused an increase of 4.44% in the debris-covered area and an increase of 0.04% in the glacial lakes. The glacier snow areas have expanded from 1990 to 2015, as evidenced by the overlaying maps of glacier surface temperature and land cover. Specifically, the glacier snow areas measured 9.56 km² compared to 7.85 km² for the colder temperature range of -19°C to -1°C , and 6.07 km² compared to 2.90 km² for 0°C . In contrast, for the warmer temperature range ($+1^{\circ}\text{C}$ to $+27^{\circ}\text{C}$), the glacier areas increased from 10.61 km² to 15.49 km². Conclusively, the more generous temperature range contained more glacier surface areas in 2015 than in 1990. The total area of the Ghulkin glacier (i.e., glacier and snow cover) underwent a marked retreat of about 1.28 km² between 1990 and 2015, with an average retreat rate of 0.05 km² per year. This is obvious from the frequent GLOF events and corresponding changes in the landscape since 1999.

The devastating GLOF trend recorded since 1999 will continue under the present climatic conditions. This research will help the local government and other stakeholders with timely and efficient monitoring of glacier lakes and associated hazards. Thus, lowland communities can be ready to adapt to the effects of climate change on the glaciers in a more effective manner.

Acknowledgments This research received funding from the USAID Partnerships for Enhanced Engagement in Research (PEER) cycle 5, under project “Satellite Enhanced Snow-Melt Flood and Drought Predictions for the Kabul River Basin with Surface and Ground Water.” The authors acknowledge the support of geologists and members of Community Watch groups (CWG) during field data collection and field analysis related to mass glacier retreats.

Credit Authorship Contribution Statement Muhammad Amin and Aqil Tariq did all the analysis and contributed equally to this chapter. All authors have read and agreed to the published version of the chapter.

Availability of Data and Material The authors would like to pay special and heart-welcoming thanks to NASA Earth data (<https://lpdaacsvc.cr.usgs.gov/appears/>) for providing the Grace satellite data. The datasets generated and/or analyzed during this study are not publicly available but are available from the corresponding author on reasonable request.

Competing Interests The authors declare that there is no conflict of interest in this chapter’s publication. Moreover, the writers have thoroughly addressed ethical issues, including plagiarism, informed consent, fraud, data manufacturing and/or falsification, dual publication and/or submission, and redundancy.

Data Availability Statement The authors would like to pay special and heart-welcoming thanks to NASA USGS (<https://earthexplorer.usgs.gov/>) for providing the Landsat data.

References

- Asif, M., Kazmi, J. H., & Tariq, A. (2023). Traditional ecological knowledge based indicators for monitoring rangeland conditions in Thal and Cholistan Desert, Pakistan. *Environmental Challenges*, *13*, 100754. <https://doi.org/10.1016/j.envc.2023.100754>
- Baloch, M. Y. J., Zhang, W., Chai, J., Li, S., Alqurashi, M., Rehman, G., Tariq, A., Talpur, S. A., Iqbal, J., Munir, M., & Hussein, E. E. (2021). Shallow groundwater quality assessment and its suitability analysis for drinking and irrigation purposes. *Water (Switzerland)*, *13*, 1–25. <https://doi.org/10.3390/w13233361>
- Baqa, M. F., Lu, L., Chen, F., Nawaz-ul-Huda, S., Pan, L., Tariq, A., Qureshi, S., Li, B., & Li, Q. (2022). Characterizing spatiotemporal variations in the urban thermal environment related to land cover changes in Karachi, Pakistan, from 2000 to 2020. *Remote Sensing*, *14*, 2164. <https://doi.org/10.3390/rs14092164>
- Basharat, M., Khan, J. A., Khalil, U., Tariq, A., Aslam, B., & Li, Q. (2022). Ensuring earthquake-proof development in a swiftly developing region through neural network modeling of earthquakes using nonlinear spatial variables. *Buildings*, *12*, 1713. <https://doi.org/10.3390/buildings12101713>
- Bera, D., Das Chatterjee, N., Mumtaz, F., Dinda, S., Ghosh, S., Zhao, N., Bera, S., & Tariq, A. (2022). Integrated influencing mechanism of potential drivers on seasonal variability of LST in Kolkata Municipal Corporation, India. *Landscape*, *11*, 1461. <https://doi.org/10.3390/land11091461>
- Bokhari, R., Shu, H., Tariq, A., Al-Ansari, N., Guluzade, R., Chen, T., Jamil, A., & Aslam, M. (2023). Land subsidence analysis using synthetic aperture radar data. *Heliyon*, *9*, e14690. <https://doi.org/10.1016/j.heliyon.2023.e14690>
- da Silva Monteiro, L., de Oliveira-Júnior, J. F., Ghaffar, B., Tariq, A., Qin, S., Mumtaz, F., Correia Filho, W. L. F., Shah, M., da Rosa Ferraz Jardim, A. M., da Silva, M. V., de Barros Santiago, D., Barros, H. G., Mendes, D., Abreu, M. C., de Souza, A., Pimentel, L. C. G., da Silva, J. L. B., Aslam, M., & Kuriqi, A. (2022). Rainfall in the urban area and its impact on climatology and population growth. *Atmosphere (Basel)*, *13*, 1610. <https://doi.org/10.3390/atmos13101610>
- Esmaili, M., Abbasi-Moghadam, D., Sharifi, A., Tariq, A., & Li, Q. (2024). ResMorCNN Model: Hyperspectral Images Classification Using Residual-Injection Morphological Features and 3DCNN Layers. *IEEE Journal of Selected Topics in Applied Earth Observations and Remote Sensing*, *17*, 219–243. <https://doi.org/10.1109/JSTARS.2023.3328389>
- Felegari, S., Sharifi, A., Moravej, K., Amin, M., Golchin, A., Muzirafuti, A., Tariq, A., & Zhao, N. (2021). Integration of Sentinel 1 and Sentinel 2 Satellite Images for Crop Mapping. *Applied Sciences*, *11*, 10104. <https://doi.org/10.3390/app112110104>
- Felegari, S., Sharifi, A., Khosravi, M., Sabanov, S., Tariq, A., & Karuppanan, S. (2023). Using Sentinel-2 data to estimate the concentration of heavy metals caused by industrial activities in Ust-Kamenogorsk, Northeastern Kazakhstan. *Heliyon*, *9*(11):e21908. <https://doi.org/10.1016/j.heliyon.2023.e21908>
- Fu, C., Cheng, L., Qin, S., Tariq, A., Liu, P., Zou, K., & Chang, L. (2022). Timely plastic-mulched cropland extraction method from complex mixed surfaces in arid regions. *Remote Sensing*, *14*, 4051. <https://doi.org/10.3390/rs14164051>
- Ghaderizadeh, S., Abbasi-Moghadam, D., Sharifi, A., Tariq, A., & Qin, S. (2022). Multiscale dual-branch residual spectral-spatial network with attention for hyperspectral image classification. *IEEE Journal of Selected Topics in Applied Earth Observations and Remote Sensing*, 1–14. <https://doi.org/10.1109/JSTARS.2022.3188732>
- Haq, S. M., Tariq, A., Li, Q., Yaqoob, U., Majeed, M., Hassan, M., Fatima, S., Kumar, M., Bussmann, R. W., Moazzam, M. F. U., & Aslam, M. (2022). Influence of edaphic properties in determining forest community patterns of the Zabarwan Mountain Range in the Kashmir Himalayas. *Forests*, *13*, 1214. <https://doi.org/10.3390/f13081214>
- Hu, P., Sharifi, A., Tahir, M. N., Tariq, A., Zhang, L., Mumtaz, F., & Shah, S. H. I. A. (2021). Evaluation of vegetation indices and phenological metrics using time-series MODIS data for

- monitoring vegetation change in Punjab, Pakistan. *Water*, *13*, 2550. <https://doi.org/10.3390/w13182550>
- Hussain, S., Lu, L., Mubeen, M., Nasim, W., Karuppanan, S., Fahad, S., Tariq, A., Mousa, B. G., Mumtaz, F., & Aslam, M. (2022a). Spatiotemporal variation in land use land cover in the response to local climate change using multispectral remote sensing data. *Landscape*, *11*, 595. <https://doi.org/10.3390/land11050595>
- Hussain, S., Qin, S., Nasim, W., Bukhari, M. A., Mubeen, M., Fahad, S., Raza, A., Abdo, H. G., Tariq, A., Mousa, B. G., Mumtaz, F., & Aslam, M. (2022b). Monitoring the dynamic changes in vegetation cover using spatio-temporal remote sensing data from 1984 to 2020. *Atmosphere (Basel)*, *13*, 1609. <https://doi.org/10.3390/atmos13101609>
- Imran, M., Ahmad, S., Sattar, A., & Tariq, A. (2022). Mapping sequences and mineral deposits in poorly exposed lithologies of inaccessible regions in Azad Jammu and Kashmir using SVM with ASTER satellite data. *Arabian Journal of Geosciences*, *15*, 538. <https://doi.org/10.1007/s12517-022-09806-9>
- Islam, F., Riaz, S., Ghaffar, B., Tariq, A., Shah, S. U., Nawaz, M., Hussain, M. L., Amin, N. U., Li, Q., Lu, L., Shah, M., & Aslam, M. (2022). Landslide susceptibility mapping (LSM) of Swat District, Hindu Kush Himalayan region of Pakistan, using GIS-based bivariate modeling. *Frontiers in Environmental Science*, *10*, 1–18. <https://doi.org/10.3389/fenvs.2022.1027423>
- Jalayer, S., Sharifi, A., Abbasi-Moghadam, D., Tariq, A., & Qin, S. (2022). Modeling and predicting land use land cover spatiotemporal changes: A case study in Chalus Watershed, Iran. *IEEE Journal of Selected Topics in Applied Earth Observations and Remote Sensing*, *15*, 5496–5513. <https://doi.org/10.1109/JSTARS.2022.3189528>
- Jalayer, S., Sharifi, A., Abbasi-Moghadam, D., Tariq, A., & Qin, S. (2023). Assessment of spatiotemporal characteristic of droughts using in situ and remote sensing-based drought indices. *IEEE Journal of Selected Topics in Applied Earth Observations and Remote Sensing*, *16*, 1483–1502. <https://doi.org/10.1109/JSTARS.2023.3237380>
- Khalil, U., Azam, U., Aslam, B., Ullah, I., Tariq, A., Li, Q., & Lu, L. (2022a). Developing a spatiotemporal model to forecast land surface temperature: A way forward for better town planning. *Sustainability*, *14*, 11873. <https://doi.org/10.3390/su141911873>
- Khalil, U., Imtiaz, I., Aslam, B., Ullah, I., Tariq, A., & Qin, S. (2022b). Comparative analysis of machine learning and multi-criteria decision making techniques for landslide susceptibility mapping of Muzaffarabad district. *Frontiers in Environmental Science*, *10*, 1–19. <https://doi.org/10.3389/fenvs.2022.1028373>
- Khan, A. M., Li, Q., Saqib, Z., Khan, N., Habib, T., Khalid, N., Majeed, M., & Tariq, A. (2022). MaxEnt modelling and impact of climate change on habitat suitability variations of economically important Chilgoza Pine (*Pinus gerardiana* Wall.) in South Asia. *Forests*, *13*, 715. <https://doi.org/10.3390/f13050715>
- Lutz, A. F., Immerzeel, W. W., Shrestha, A. B., & Bierkens, M. F. P. (2014). Consistent increase in High Asia's runoff due to increasing glacier melt and precipitation. *Nature Climate Change*, *4*, 587–592. <https://doi.org/10.1038/nclimate2237>
- Majeed, M., Tariq, A., Anwar, M. M., Khan, A. M., Arshad, F., Mumtaz, F., Farhan, M., Zhang, L., Zafar, A., Aziz, M., Abbasi, S., Rahman, G., Hussain, S., Waheed, M., Fatima, K., & Shaukat, S. (2021). Monitoring of land use–Land cover change and potential causal factors of climate change in Jhelum district, Punjab, Pakistan, through GIS and multi-temporal satellite data. *Landscape*, *10*. <https://doi.org/10.3390/land10101026>
- Majeed, M., Lu, L., Haq, S. M., Waheed, M., Sahito, H. A., Fatima, S., Aziz, R., Bussmann, R. W., Tariq, A., Ullah, I., & Aslam, M. (2022a). Spatiotemporal distribution patterns of climbers along an abiotic gradient in Jhelum District, Punjab, Pakistan. *Forests*, *13*, 1244. <https://doi.org/10.3390/f13081244>
- Majeed, M., Tariq, A., Haq, S. M., Waheed, M., Anwar, M. M., Li, Q., Aslam, M., Abbasi, S., Mousa, B. G., & Jamil, A. (2022b). A detailed ecological exploration of the distribution patterns of wild Poaceae from the Jhelum District (Punjab), Pakistan. *Sustainability*, *14*, 3786. <https://doi.org/10.3390/su14073786>

- Majeed, M., Lu, L., Anwar, M. M., Tariq, A., Qin, S., El-Hefnawy, M. E., El-Sharnouby, M., Li, Q., & Alasmari, A. (2023). Prediction of flash flood susceptibility using integrating analytic hierarchy process (AHP) and frequency ratio (FR) algorithms. *Frontiers in Environmental Science*, 10, 1–14. <https://doi.org/10.3389/fenvs.2022.1037547>
- Mihalcea, C., Mayer, C., Diolaiuti, G., D'Agata, C., Smiraglia, C., Lambrecht, A., Vuillermoz, E., & Tartari, G. (2008). Spatial distribution of debris thickness and melting from remote-sensing and meteorological data, at debris-covered Baltoro glacier, Karakoram, Pakistan. In *Annals of glaciology* (pp. 49–57). <https://doi.org/10.3189/172756408784700680>
- Moazzam, M. F. U., Rahman, G., Munawar, S., Tariq, A., Safdar, Q., & Lee, B. (2022). Trends of rainfall variability and drought monitoring using standardized precipitation index in a scarcely gauged basin of Northern Pakistan. *Water*, 14, 1132. <https://doi.org/10.3390/w14071132>
- Mousa, B. G., Shu, H., Freeshah, M., & Tariq, A. (2020). A novel scheme for merging active and passive satellite soil moisture retrievals based on maximizing the signal to noise ratio. *Remote Sensing*, 12, 1–23. <https://doi.org/10.3390/rs12223804>
- Pimentel, S., & Flowers, G. E. (2011). A numerical study of hydrologically driven glacier dynamics and subglacial flooding. In *Proceedings of the Royal Society A: Mathematical, Physical and Engineering Sciences* (pp. 537–558). The Royal Society Publishing. <https://doi.org/10.1098/rspa.2010.0211>
- Quincey, D. J., & Luckman, A. (2014). Brief communication: On the magnitude and frequency of Khurdopin glacier surge events. *The Cryosphere*, 8, 571–574. <https://doi.org/10.5194/tc-8-571-2014>
- Quincey, D. J., Copland, L., Mayer, C., Bishop, M., Luckman, A., & Belò, M. (2009). Ice velocity and climate variations for Baltoro Glacier, Pakistan. *Journal of Glaciology*, 55, 1061–1071. <https://doi.org/10.3189/002214309790794913>
- Quincey, D. J., Braun, M., Glasser, N. F., Bishop, M. P., Hewitt, K., & Luckman, A. (2011). Karakoram glacier surge dynamics. *Geophysical Research Letters*, 38, 2–7. <https://doi.org/10.1029/2011GL049004>
- Round, V., Leinss, S., Huss, M., Haemmig, C., & Hajnsek, I. (2017). Surge dynamics and lake outbursts of Kyagar Glacier, Karakoram. *The Cryosphere*, 11, 723–739. <https://doi.org/10.5194/tc-11-723-2017>
- Shah, S. H. I. A., Yan, J., Ullah, I., Aslam, B., Tariq, A., Zhang, L., & Mumtaz, F. (2021). Classification of aquifer vulnerability by using the DRASTIC index and geo-electrical techniques. *Water*, 13, 2144. <https://doi.org/10.3390/w13162144>
- Shah, S. H. I. A., Jianguo, Y., Jahangir, Z., Tariq, A., & Aslam, B. (2022). Integrated geophysical technique for groundwater salinity delineation, an approach to agriculture sustainability for Nankana Sahib Area, Pakistan. *Geomatics, Natural Hazards And Risk*, 13, 1043–1064. <https://doi.org/10.1080/19475705.2022.2063077>
- Sharifi, A., Felegari, S., Tariq, A., & Siddiqui, S. (2021). Forest cover change detection across recent three decades in Persian oak forests using convolutional neural network. In *Climate impacts on sustainable natural resource management* (pp. 57–73). Wiley. <https://doi.org/10.1002/9781119793403.ch4>
- Sharifi, A., Felegari, S., & Tariq, A. (2022a). Mangrove forests mapping using Sentinel-1 and Sentinel-2 satellite images. *Arabian Journal of Geosciences*, 15, 1593. <https://doi.org/10.1007/s12517-022-10867-z>
- Sharifi, A., Mahdipour, H., Moradi, E., & Tariq, A. (2022b). Agricultural field extraction with deep learning algorithm and satellite imagery. *Journal of the Indian Society of Remote Sensing*, 50, 417–423. <https://doi.org/10.1007/s12524-021-01475-7>
- Siddiqui, S., Ali Safi, M. W., Rehman, N. U., & Tariq, A. (2020). Impact of climate change on land use/land cover of Chakwal District. *International Journal of Economic and Environmental Geology*, 11, 65–68. <https://doi.org/10.46660/ijeeg.vol11.iss2.2020.449>
- Tariq, A. (2023). Quantitative comparison of geostatistical analysis of interpolation techniques and semivariogram spatial dependency parameters for soil atrazine contamination attribute. In: Stathopoulos N, Tsatsaris A, Kalogeropoulos KBT-G for G (eds) *Geoinformatics for Geosciences*. Elsevier, pp 261–279

- Tariq, A., & Qin, S. (2023). Spatio-temporal variation in surface water in Punjab, Pakistan from 1985 to 2020 using machine-learning methods with time-series remote sensing data and driving factors. *Agricultural Water Management*, 280, 108228. <https://doi.org/10.1016/j.agwat.2023.108228>
- Tariq, A., & Shu, H. (2020). CA-Markov chain analysis of seasonal land surface temperature and land use landcover change using optical multi-temporal satellite data of Faisalabad, Pakistan. *Remote Sensing*, 12, 1–23. <https://doi.org/10.3390/rs12203402>
- Tariq, A., Mumtaz, F., Zeng, X., Baloch, M. Y. J., & Moazzam, M. F. U. (2022a). Spatio-temporal variation of seasonal heat islands mapping of Pakistan during 2000–2019, using day-time and night-time land surface temperatures MODIS and meteorological stations data. *Remote Sensing Applications: Society and Environment*, 27, 100779. <https://doi.org/10.1016/j.rsase.2022.100779>
- Tariq, A., Siddiqui, S., Sharifi, A., & Shah, S. H. I. A. (2022b). Impact of spatio-temporal land surface temperature on cropping pattern and land use and land cover changes using satellite imagery, Hafizabad District, Punjab, Province of Pakistan. *Arabian Journal of Geosciences*, 15, 1045. <https://doi.org/10.1007/s12517-022-10238-8>
- Tariq, A., Yan, J., Gagnon, A. S., Riaz Khan, M., & Mumtaz, F. (2022c). Mapping of cropland, cropping patterns and crop types by combining optical remote sensing images with decision tree classifier and random forest. *Geo-spatial Information Science*, 00, 1–19. <https://doi.org/10.1080/10095020.2022.2100287>
- Tariq, A., Yan, J., Ghaffar, B., Qin, S., Mousa, B. G., Sharifi, A., Huq, M. E., & Aslam, M. (2022d). Flash flood susceptibility assessment and zonation by integrating analytic hierarchy process and frequency ratio model with diverse spatial data. *Water*, 14, 3069. <https://doi.org/10.3390/w14193069>
- Tariq, A., Hashemi Beni, L., Ali, S., et al. (2023). An effective geospatial-based flash flood susceptibility assessment with hydrogeomorphic responses on groundwater recharge. *Groundwater for Sustainable Development*, 5, 100998. <https://doi.org/10.1016/j.gsd.2023.100998>
- Tariq, A., Jiango, Y., Li, Q., Gao, J., Lu, L., Soufan, W., Almutairi, K. F., & Habib-ur-Rahman, M. (2023a). Modelling, mapping and monitoring of forest cover changes, using support vector machine, kernel logistic regression and naive Bayes tree models with optical remote sensing data. *Heliyon*, 9, e13212. <https://doi.org/10.1016/j.heliyon.2023.e13212>
- Tariq, A., Jiango, Y., Lu, L., Jamil, A., Al-ashkar, I., Kamran, M., & El Sabagh, A. (2023b). Integrated use of Sentinel-1 and Sentinel-2 data and open-source machine learning algorithms for burnt and unburnt scars. *Geomatics, Natural Hazards and Risk*, 14, 28. <https://doi.org/10.1080/19475705.2023.2190856>
- Ullah, I., Aslam, B., Shah, S. H. I. A., Tariq, A., Qin, S., Majeed, M., & Havenith, H.-B. (2022). An integrated approach of machine learning, remote sensing, and GIS data for the landslide susceptibility mapping. *Landscape*, 11, 1265. <https://doi.org/10.3390/land11081265>
- Wahla, S. S., Kazmi, J. H., Sharifi, A., Shirazi, S. A., Tariq, A., & Joyell Smith, H. (2022). Assessing spatio-temporal mapping and monitoring of climatic variability using SPEI and RF machine learning models. *Geocarto International*, 0, 1–20. <https://doi.org/10.1080/10106049.2022.2093411>
- Zamani, A., Sharifi, A., Felegari, S., Tariq, A., & Zhao, N. (2022). Agro climatic zoning of saffron culture in Miyaneh City by using WLC method and remote sensing data. *Agriculture*, 12, 1–15. <https://doi.org/10.3390/agriculture12010118>